Acta Pharmacologica Sinica (2017) 38: 907–913
 1671-4083/17
www.nature.com/aps

Original Article

Intrinsic radiolabeling of Titanium-45 using mesoporous silica nanoparticles

Feng CHEN[1, #], Hector F VALDOVINOS[2, #], Reinier HERNANDEZ[2], Shreya GOEL[3], Todd E BARNHART[2], Weibo CAI[1, 2, 3, 4, *]

[1]Department of Radiology, University of Wisconsin-Madison, WI, USA; [2]Department of Medical Physics, University of Wisconsin-Madison, WI, USA; [3]Materials Science Program, University of Wisconsin-Madison, WI, USA; [4]University of Wisconsin Carbone Cancer Center, Madison, WI, USA

Abstract

Titanium-45 (^{45}Ti) with a three-hour half-life ($t_{1/2}$=3.08 h), low maximum positron energy and high positron emission branching ratio, is a suitable positron emission tomography (PET) isotope whose potential has not yet been fully explored. Complicated radiochemistry and rapid hydrolysis continue to be major challenges to the development of ^{45}Ti compounds based on a traditional chelator-based radiolabeling strategy. In this study we introduced an intrinsic (or chelator-free) radiolabeling technique for the successful labeling of ^{45}Ti using mesoporous silica nanoparticle (MSN). We synthesized uniform MSN with an average particle size of ~150 nm in diameter. The intrinsic ^{45}Ti-labeling was accomplished through strong interactions between ^{45}Ti (hard Lewis acid) and hard oxygen donors (hard Lewis bases), the deprotonated silanol groups (-Si-O-) from the outer surface and inner meso-channels of MSN. *In vivo* tumor-targeted PET imaging of as-developed PEGylated [^{45}Ti]MSN was further demonstrated in the 4T1 murine breast tumor-bearing mice. This MSN-based intrinsic radiolabeling strategy could open up new possibilities and speed up the biomedical applications of ^{45}Ti in the future.

Keywords: positron emission tomography; titanium-45; intrinsic radiolabeling; mesoporous silica nanoparticle; tumor targeting; 4T1 murine breast tumor

Acta Pharmacologica Sinica (2017) 38: 907–913; doi: 10.1038/aps.2017.1; published online Apr 17 2017

Introduction

Positron Emission Tomography (PET) is a highly quantitative, whole body functional imaging technique that plays a vital role in model clinical diagnosis and pre-clinical research[1]. During PET imaging, a radionuclide (or probe) produces positrons, which annihilate with surrounding electrons to release two 511 keV photons in opposing directions. The detectors of the PET scanner measure these photons and use this information to create an image of the probe distribution in the body. To date, positron emission radioisotopes, such as fluorine-18 (^{18}F, $t_{1/2}$=109.8 min), copper-64 (^{64}Cu, $t_{1/2}$=12.7 h), and zirconium-89 (^{89}Zr, $t_{1/2}$=78.4 h), have been actively used for clinical use and translational and pre-clinical research[2].

Most current radiolabeling involves the use of exogenous chelators, which coordinate with radioisotopes to form a stable complex[3]. Nanoparticle-based intrinsic radiolabeling is an emerging chelator-free radiolabeling technique that takes advantages of the physical and chemical properties of both the nanoparticle and the selected radioisotopes[4, 5]. Successful labeling of isotopes, such as ^{64}Cu, arsenic-72 (^{72}As, $t_{1/2}$=26 h), germanium-69 (^{69}Ge, $t_{1/2}$=39.1 h) and ^{89}Zr, using this technique has recently been achieved by us and other groups[6–13].

Titanium-45 (^{45}Ti, $t_{1/2}$=3.08 h), with a 3-h half-life, low maximum positron energy (E_{max}=1040 keV, E_{avg}=439 keV) and high branching ratio (β^+=84.8%), is a suitable PET isotope whose potential has not yet been fully explored due to challenges in achieving stable radiolabeling. Although it is relatively easy to generate on a cyclotron, its complicated radiochemistry and rapid oxidation of the metal in aqueous solution[14] have resulted in few beingliterature reports during the last three decades on the radiolabeling and biomedical application of ^{45}Ti[15–20]. For example, one of the very first ^{45}Ti labeling studies was reported more than 30 years ago, when the ^{45}Ti-titanium ascorbate complex (^{45}Ti-AsA) was synthesized for tracking ^{45}Ti in plants and live animals[16]. A doubly labeled complex was also prepared from ^{14}C-ascorbic acid to form ^{45}Ti-AsA-^{14}C. Autoradiogram imaging in an osteogenic-disordered rat demonstrated that the ^{45}Ti-AsA distribution did not coincide with that of ^{45}Ti-AsA-^{14}C, a clear indication of the low *in vivo*

# These authors contributed equally to this work.
*To whom correspondence should be addressed.
E-mail wcai@uwhealth.org
Received 2016-11-12 Accepted 2017-02-04

radiostability of the ^{45}Ti-AsA complex[16].

In a follow-up study by Ishiwata *et al*, four ^{45}Ti-labeled compounds, ^{45}Ti-labeled phytate (^{45}TiO-phytate), ^{45}Ti-labeled human serum albumin (^{45}TiO-HAS), ^{45}Ti-labeled diethylenetriaminepentaacetic acid (^{45}TiO-DTPA), and ^{45}Ti-labeled citric acid (^{45}TiO-CA), were developed and tested in male Donryu rats[17]. Given large colloid formation, $^{45}TiOCl_2$ and ^{45}TiO-phytate shared a similar biodistribution pattern with high uptake in liver, spleen and lungs. In contrast, the remaining three ^{45}Ti compounds (*ie*, ^{45}TiO-DTPA, ^{45}TiO-HAS and ^{45}TiO-CA) showed similar tissue distributions, with high blood activity and low uptake in the reticuloendothelial system (RES). Further plasma protein binding and *in vivo* tumor targeting studies provided evidence of DTPA dissociation from the ^{45}TiO-DTPA compound and the strong binding of free ^{45}Ti with transferrin in the plasma. It was concluded that ^{45}TiO-phytate could be used for imaging the RES, whereas ^{45}TiO-DTPA has the potential for measuring blood volume or as a blood-brain-barrier indicator.

Perhaps inspired by Ishiwata's work, very recently, Vavere and co-workers reported a more systematic investigation on the *in vivo* biodistribution of ^{45}Ti-transferrin, aiming to provide deeper insight into the mechanism of action of titanocene dichloride (a chemotherapeutic agent currently in clinical trials)[19]. ^{45}Ti-Transferrin was prepared by re-dissolving the processed ^{45}Ti in apotransferrin or by *in vivo* incorporation through the introduction of ^{45}Ti-citrate. Similar biodistribution patterns and *in vivo* tumor (EMT-6, expresses high levels of transferrin receptors) uptakes were observed when directly injecting ^{45}Ti-transferrin and ^{45}Ti-citrate, which could transchelate to transferrin before the time of imaging. Despite these previous efforts, no attempts have been made to date using nanoparticles for the radiolabeling of ^{45}Ti.

Here, we introduce a mesoporous silica nanoparticle (MSN, a highly attractive, widely studied drug delivery nanoplatform[21, 22])-based intrinsic ^{45}Ti radiolabeling technique and investigate the potential of PEGylated [^{45}Ti]MSN for *in vivo* tumor passively targeted PET imaging.

Materials and methods

Synthesis of mesoporous silica nanoparticles (MSN)

In a typical synthesis of ~150 nm sized MSN with 4- to 5-nm pore size, 24 mL of hexadecyl trimethyl ammonium chloride (CTAC, 25 wt%) solution and 0.18 g of triethylamine (TEA) were added to 36 mL of water and stirred gently at 60 °C for 3 h in a 100-mL round bottom flask. Twenty mL of (20% *v/v*) tetraethyl orthosilicate (TEOS) in cyclohexane was carefully added to the water-CTAC-TEA solution and incubated at 60 °C in a water bath for 12 h (stirring rate was set to 125 r/min). Afterwards, milky white samples were collected by centrifugation (at 12500×*g* for 10 min). The samples were subjected to CTAC removal process by stirring in 1 wt% NaCl/methanol solution 3 times (24 h/time).

To functionalize the MSN surface with -NH_2 groups, as-synthesized MSN was first dispersed in 20 mL of absolute ethanol followed by the addition of 1 mL of (3-aminopropyl) triethoxysilane (APS). The system was sealed and maintained at 86 to 90 °C in a water bath for 24 h. Afterward, the mixture was centrifuged and washed with ethanol several times to remove the residual APS. The MSN-NH_2 was well dispersed in water, and the concentration of -NH_2 groups (nmol/mL) was measured using a Kaiser test kit.

Synthesis of dense silica nanoparticles ($dSiO_2$)

In a typical synthesis of uniform ~90 nm sized $dSiO_2$, 35.7 mL of absolute ethanol was mixed with 5 mL of water and 0.8 mL of ammonia and stirred for 5 to 10 min at room temperature. One mL of TEOS was then added, and the mixture was allowed to react at room temperature for 1 h. Afterward, $dSiO_2$ nanoparticles were collected by centrifugation (at 12500×*g* for 10 min), washed with water/ethanol 3 times, and re-suspended in 20 mL of water before use.

Synthesis of sodium citrate-capped CuS nanoparticles (CuS-Cit)

Previously reported procedures were used for the synthesis of CuS-Cit with slight modifications[23, 24]. For a typical synthesis, 10 mL of $CuCl_2$ water solution (0.85 mg/mL) and 10 mL of sodium citrate (1.0 mg/mL) were added to 30 mL water. The mixture was stirred for 30 min at room temperature. After that, 50 μL Na_2S (60.54 mg/250 μL) was added to the mixture and stirred for an additional 5 min before transferring to a 90 °C water bath. The reaction was incubated for 15 min before cooling down with ice, forming green-colored CuS-Cit nanoparticles.

Synthesis of [^{45}Ti]MSN-PEG_{5k}

MSN was first labeled with ^{45}Ti using the procedures previously described by incubating ^{45}Ti with MSN-NH_2 for one hour at pH 7–8 and 75 °C. The sample was then collected by centrifugation (at 12500×*g* for 10 min) and washed with water 3 times. Then, a well-established PEGylation process was introduced by reacting [^{45}Ti]MSN-NH_2 with 5 mg (1000 nmol) of SCM-PEG_{5k}-Mal in pH 7 for 60 min. The PEGylated sample was isolated by centrifugation at 12500×*g* for 10 min. Free PEG was removed by washing with PBS at least 2 times. As synthesized [^{45}Ti]MSN-PEG_{5k} was then used for *in vivo* passively targeted tumor imaging.

4T1 tumor model

To generate the 4T1 tumor model, 4- to 5-week-old female BALB/c mice were purchased from Harlan (Indianapolis, IN, USA), and tumors were established by subcutaneously injecting 2×10^6 cells suspended in 100 μL of 1:1 mixture of RPMI-1640 and Matrigel (BD Biosciences, Franklin Lakes, NJ, USA) into the front flank of mice. The tumor sizes were monitored every other day, and the animals were subjected to *in vivo* experiments when the tumor diameter reached 5 to 8 mm.

In vivo PET imaging

All animal studies were conducted under a protocol approved by the University of Wisconsin Institutional Animal Care and Use Committee. PET scans at various time points post-

injection (pi) using a microPET/microCT Inveon rodent model scanner (Siemens Medical Solutions, USA, Inc), image reconstruction, and region-of-interest (ROI) analysis of the PET data were performed as previously described[25]. Quantitative PET data were presented as percentage injected dose per gram of tissue (%ID/g). 4T1 murine breast tumor-bearing mice, a fast-growing tumor model, were each intravenously injected with ~300 μCi (or 11.1 MBq) [^{45}Ti]MSN-PEG$_{5k}$ or free ^{45}Ti (diluted with PBS) before serial PET scans.

Ex vivo biodistribution study

Biodistribution studies were performed to confirm that the %ID/g values based on PET imaging truly represented the radioactivity distribution in tumor-bearing mice. Mice were euthanized, and blood, 4T1 tumor, and major organs/tissues were collected and wet-weighed. The radioactivity in the tissue was measured using a gamma-counter (Perkin-Elmer) and presented as%ID/g (%ID/g=percentage injected dose per gram, mean±SD).

Results and discussion

Generation and characterizations of titanium-45

^{45}Ti was produced by proton irradiation of a 0.25-mm-thick scandium foil (99.9%, 96–140 mg) with a current of 20 μA on a GE PETtrace. A 254-μm niobium degrader was used to reduce the proton energy from the nominal 16.0 MeV to 11.8 MeV to avoid the production of ^{44}Ti from ^{45}Sc(p,2n). During irradiation, heat from the scandium foil was removed by contact with a water-cooled silver disk. The activated foil was dissolved in 3 to 4 mL of 6 mol/L HCl. The solution was then diluted with 18 MΩ·cm water (2 to 4 mL) to a concentration of ~2 mol/L HCl.

The separation of ^{45}Ti was performed on a hydroxamic acid resin[26]. Briefly, the hydroxamic acid resin was prepared and equilibrated with 2 mol/L HCl[27]. The target dissolution in 2 mol/L HCl (5 to 8 mL) was passed at a flow rate of 1.1 mL/min over 100 mg of resin loaded in a 5-mm-diameter column using the peristaltic pump-driven, automated module[28]. Upon passing the target solution through the column, a wash of 5 mL of 2 mol/L HCl was passed before elution with 1 mol/L oxalic acid in fractions of 200 μL. The entire separation process required approximately one hour. The radionuclidic purity assay employed a high-purity germanium (HPGe) detector (Canberra C1519) and an ion chamber (Capintec) connected to an electrometer (Keithley 6517A) for decay logging. MicroPET images of a Derenzo phantom were also obtained for resolution evaluation.

Results showed that one-hour irradiations generate 4.6±0.4 GBq of ^{45}Ti (n=6). In addition, 42%±6% of this activity was separated in 600 μL of 1 mol/L oxalic acid. The gamma spectrum (Figure 1A) obtained with the HPGe detector exhibited expected 511 keV photons and the two characteristic gammas from ^{45}Ti at 720 and 1408 keV after a 2.3-h assay, as shown in Figure 1B and 1C. A single exponential fit to the data from the decay logging indicated that the half-life of the separated radionuclide is 3.067±0.004 h, which is only 0.4% less than

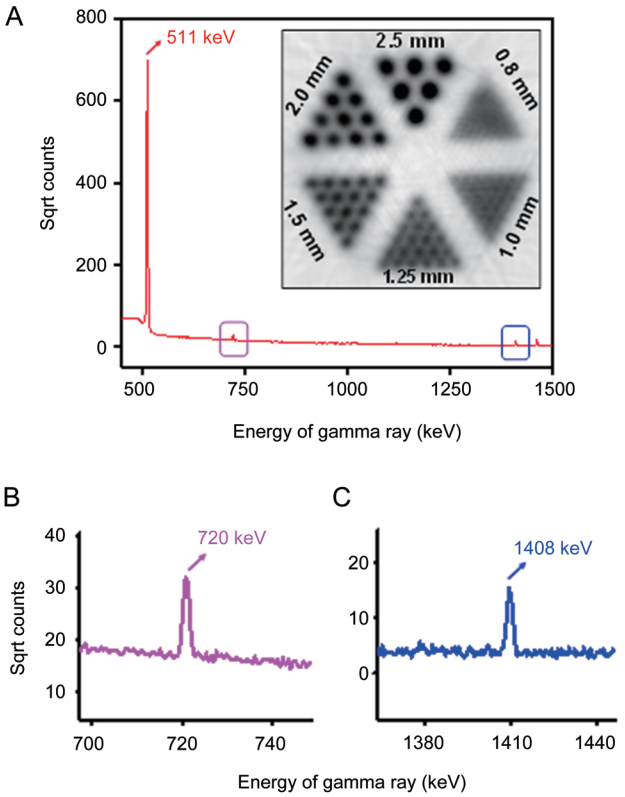

Figure 1. Generation and characterization of Titanium-45. (A) A gamma spectrum of ^{45}Ti obtained with the HPGe detector. (B and C) show the enlarged spectra of two characteristic gammas from ^{45}Ti at 720 and 1408 keV (pointed by link and blue arrows). Inset in (A) shows the MicroPET image of a Derenzo phantom of ^{45}Ti. The distance values shown in the phantom image are the diameters of the cylinders in each region. The distance between axes of the cylinders is twice their diameter.

the value reported in the National Nuclear Data Center[29]. MicroPET images of a miniature Derenzo phantom exhibited excellent resolution down to a rod diameter of 2 mm (Figure 1A, inset).

MSN-based intrinsic radiolabeling of titanium-45

Uniform MSN with an average particle size of ~150 nm in diameter was synthesized using previously reported procedures (Figure 2A)[9, 30]. The Brunauer-Emmett-Teller (BET) surface area of as-synthesized MSN was 581.5 m^2/g, with a high pore volume of 1.36 cm^3/g and an average pore size of 4 to 5 nm. Approximately 2.6×10^6 -Si-OH groups in each MSN particle was estimated based on our previous calculation[9].

Previously, we reported the successful chelator-free radiolabeling of ^{89}Zr to the abundant deprotonated silanol groups (-Si-O$^-$) from MSN[9]. Like ^{89}Zr^{4+}, ^{45}Ti^{4+} is also a hard Lewis acid and thus prefers hard Lewis bases, such as -Si-O$^-$, as the donor groups (Figure 2B). To demonstrate this feature, we mixed 250 μL of MSN (2 mg/mL) with 0.5 mCi (or 18.5 MBq) ^{45}Ti-oxalate, and the solution was shaken under varied labeling conditions. Approximately 80% labeling yield was achieved within 30 min of incubating at 75 °C, pH 7–8 (Figure 3A, black

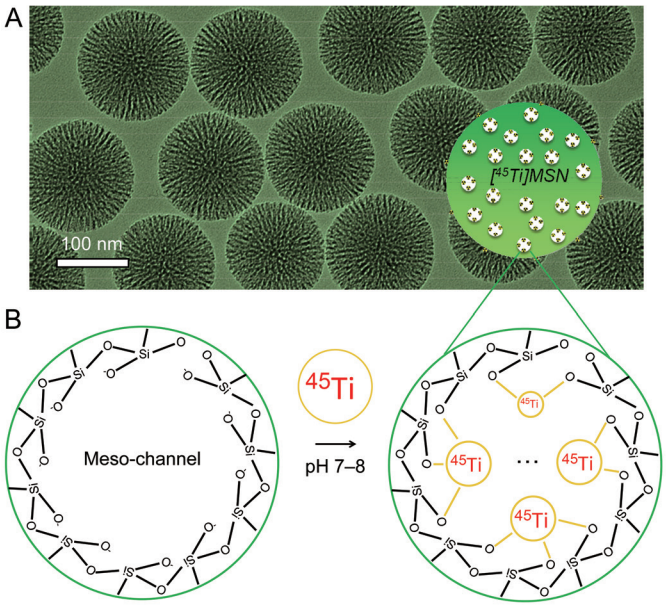

Figure 2. Synthesis and characterization of MSN. (A) A transmission electron microscopy (TEM) image of ~150 nm sized MSN particles. Surface area: 581.5 m^2/g. Pore volume: 1.36 cm^3/g. Average pore size: 4–5 nm. (B) A schematic illustration showing the labeling of ^{45}Ti to the deprotonated silanol groups (-Si-O-) from the outer surface and inner meso-channels of MSN. Please note the real coordination chemistry of $^{45}Ti^{4+}$ with the silanol groups could be much more complex than the scheme shown in (B).

line). The labeling yield further increased to ~90% after an additional 30-min incubation, which was confirmed by the radio-iTLC study (Figure 3B). As expected, a significantly reduced labeling yield (~25%) was observed when labeling was performed at pH 2–3 (75 °C), indicating the inhibition of ^{45}Ti labeling if -Si-O^- groups become protonated (Figure 3, left, red line). Such protonation was also confirmed by the surface charge change of MSN from -48.4±0.3 mV (pH 7–8) to 3.6±0.3 mV (pH 2–3).

To further demonstrate the specific labeling of ^{45}Ti to the deprotonated silanol groups, dense silica nanoparticles ($dSiO_2$) and copper sulfide (CuS) nanoparticles with less (~1.5×10^5 -Si-O^- per $dSiO_2$)[9] or almost no oxygen donors were introduced as control groups. Our results revealed ~60% and <10% labeling yield under the optimized labeling conditions (pH 7–8, 75 °C, 60 min, Figure 3, left, pink and green lines) for $dSiO_2$ and CuS, respectively, clearly demonstrating the -Si-O^--dependent ^{45}Ti labeling process. More detailed labeling yields and autoradiography images are presented in Figure S1 (Supporting Information). Given that the intrinsic ^{45}Ti-labeling mechanism is based on the strong interaction between ^{45}Ti (hard Lewis acid) and hard oxygen donors (hard Lewis bases), successful chelator-free ^{45}Ti radiolabeling might also be achievable using other oxygen-containing nanoparticles. This finding was confirmed by successful chelator-free ^{45}Ti labeling to water-soluble SPION@PAA [SPION: superparamagnetic iron oxide nanoparticle, PAA: poly(acrylic acid)], as shown in Figure S2.

In vivo tumor-targeted PET Imaging

An *in vitro* serum stability study was performed prior to the *in vivo* ^{45}Ti-based PET imaging. The *in vitro* radiostability of [^{45}Ti]MSN was less stable than that of [^{89}Zr]MSN[9]. As shown in Figure S3, approximately 15% of ^{45}Ti was detached from the [^{45}Ti]MSN after incubated in mouse serum at 37 °C for 3 h. Approximately 20% of detached free ^{45}Ti was observed within 14 h (more than 4 half-lives of ^{45}Ti).

To demonstrate the feasibility of using ^{45}Ti-labeled MSN for *in vivo* tumor-targeted PET imaging, the nanoparticle was first modified with -NH_2 groups and then labeled with ^{45}Ti (pH 7–8, 75 °C) followed by a well-established PEGylation step[9]. Surface PEGylation provides significantly improved nanoparticle stability in biological buffers and *in vivo* and does not

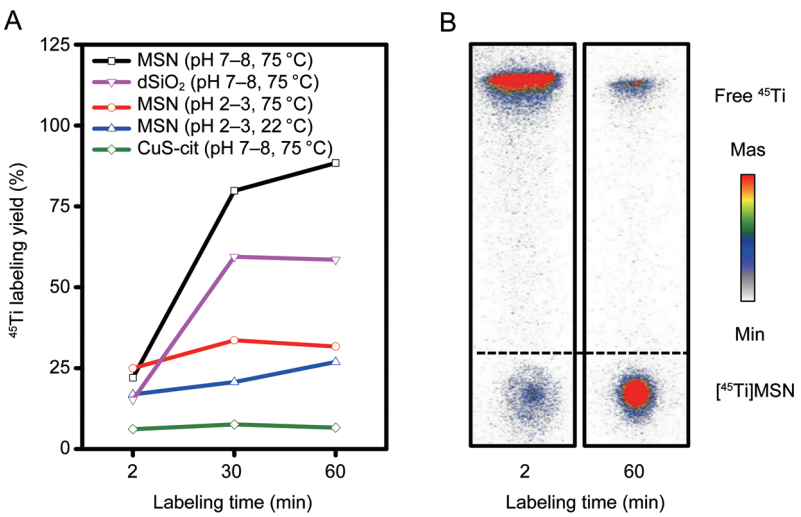

Figure 3. MSN-based intrinsic radiolabeling of titanium-45. (A) ^{45}Ti labeling yields of different samples under varied labeling conditions. (B) An autoradiograph of [^{45}Ti]MSN iTLC plates after 2 min and 60 min incubation (pH 7–8, 75 °C).

affect the labeling of ^{45}Ti due to the abundant silanol groups in each MSN particles (especially those inside the meso-channels). The blood circulation half-life ($t_{1/2}$) of PEGylated MSN was estimated to be approximately 4 h, which was very close to the decay half-life of ^{45}Ti ($t_{1/2}$=3.08 h), but significantly longer than that of the same sample with no PEG protective layer ($t_{1/2}$<10 min). Synthesized [^{45}Ti]MSN-PEG$_{5k}$ was then intravenously injected to 4T1 murine breast tumor-bearing mice. To compare the biodistribution patterns between the free ^{45}Ti and [^{45}Ti]MSN-PEG$_{5k}$ (HD: ~200 nm), we further injected free ^{45}Ti-oxalate (diluted with PBS, pH 7.4) into another group of 4T1 murine breast tumor-bearing mice and compared organ uptake over time.

The PET imaging in Figure 4 clearly revealed differences in biodistribution at 30 min post-injection. As expected, mice injected with [^{45}Ti]MSN-PEG$_{5k}$ shared a similar PK (dominant uptake in liver [43.2%±6.6% ID/g] and heart [16.7%±2.6% ID/g]) compared with that injected with our previously reported ^{89}Zr chelator-free labeled MSN-PEG$_{5k}$[31]. Mice injected with free ^{45}Ti exhibited a significantly different PK, with an approximately two-fold increased uptake in the blood (31.9%±8.8% ID/g) and a two-fold reduced uptake in the liver (22.3%±3.0% ID/g). Interestingly, cold Ti and radioactive ^{45}Ti have a strong interaction with unsaturated transferrin in mouse (or human) blood, where transferrin could act as a mediator for titanium delivery to tumor cells[19, 32, 33]. Like ^{45}Ti-citrate[19], ^{45}Ti-oxalate was expected to transchelate to transferrin to form ^{45}Ti-transferrin *in vivo*. These features explain the high initial blood retention of free ^{45}Ti. The tumor uptake of [^{45}Ti]MSN-PEG$_{5k}$ at 30 min pi was approximately 1.7% ID/g, which is approximately half of that in mice injected with free ^{45}Ti (Figure 4). Possibly due to the longer blood circulation

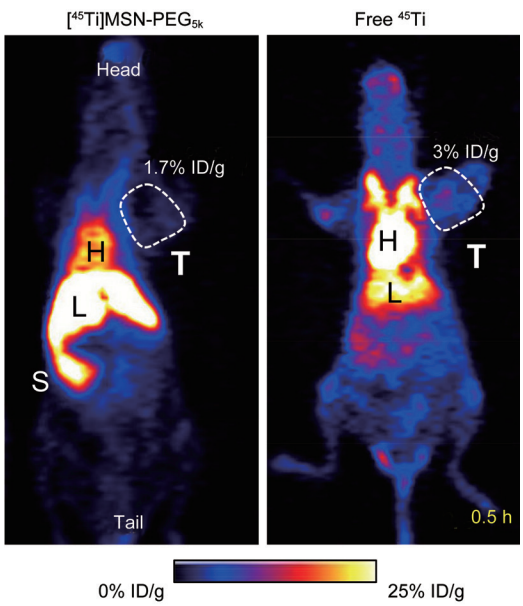

Figure 4. Comparison of the *in vivo* biodistribution between [^{45}Ti]MSN-PEG$_{5k}$ (Left) and free ^{45}Ti (Right) at early time point (0.5 h post-injection) by using PET imaging. H: heart; L: liver; S: spleen; T: tumor.

half-life of ^{45}Ti-transferrin, mice injected with free ^{45}Ti exhibited significantly increased tumor accumulation over time (from 3.0%±0.3% ID/g at 0.5 h pi to 14.3%±0.9% ID/g at 14 h *pi*), as shown in Figure 5A, 5B and Table S1.

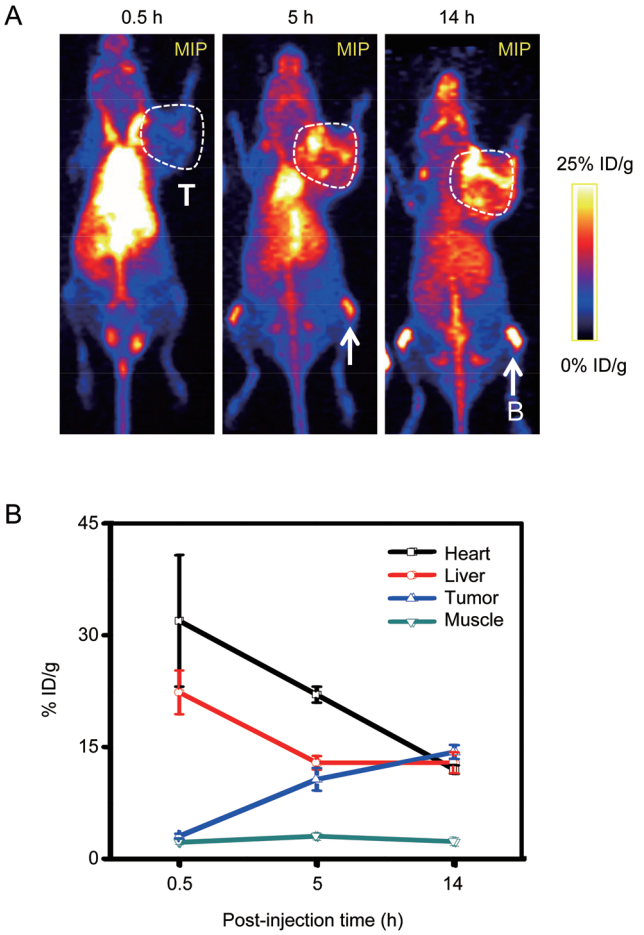

Figure 5. (A) *In vivo* serial coronal maximum intensity projection (MIP) PET images of 4T1 tumor-bearing mice (n=3) injected with free ^{45}Ti. Tumor (T) was marked with a white box. Bone (B) uptake was indicated with white arrows. (B) Time-activity curves of heart, liver, tumor and muscle.

For mice injected with [^{45}Ti]MSN-PEG$_{5k}$, our region-of-interest (ROI) quantification revealed reduced heart uptake (from 16.7%±2.6% ID/g to 7.4%±1.8% ID/g) and increased tumor uptake (from 1.7%±0.3% ID/g to 4.6%±1.4% ID/g, Figure 6, Table S2). The accumulation of [^{45}Ti]MSN-PEG$_{5k}$ is primarily based on the well-known enhanced permeability and retention effect[34]. The liver uptake was maintained at constant levels at approximately 44% ID/g, which also indicates the high radio-stability of [^{45}Ti]MSN-PEG$_{5k}$ *in vivo*. Similar tumor (~4% ID/g) and high liver uptake (50%–60% ID/g) were observed for ^{89}Zr chelator-free labeled MSN-PEG$_{5k}$[31]. A medium level (4.4%±1.9% ID/g) of bone uptake was also observed based on the maximum intensity projection (MIP) PET images (Figure 6B, pointed by white arrows) and *ex vivo* biodistribution

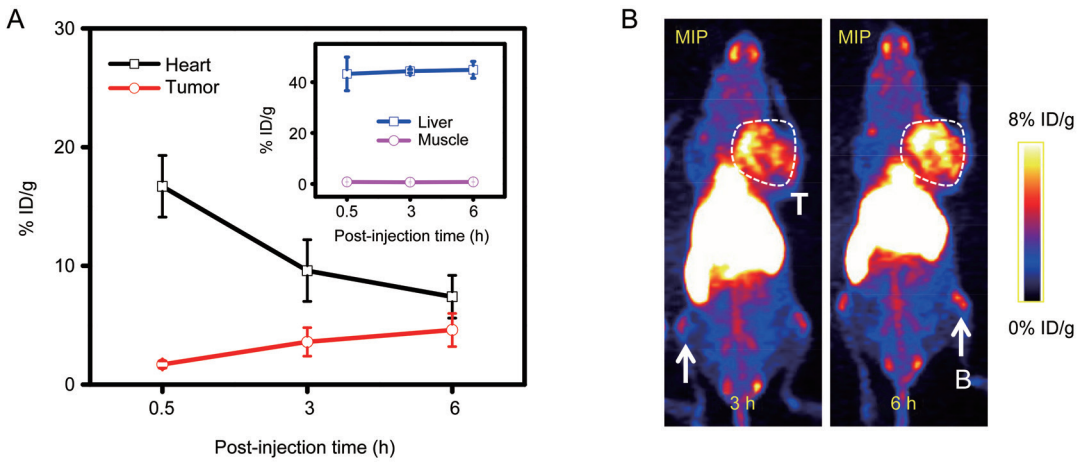

Figure 6. (A) Time-activity curves. (B) *In vivo* serial coronal maximum intensity projection PET images of 4T1 tumor-bearing mice injected with [^{45}Ti]MSN-PEG$_{5k}$. Tumor (T) was marked with a white box. Bone (B) uptake was indicated with white arrows.

study (Figure 7, Table S3). However, significantly increased bone and joint uptakes were observed in mice injected with free ^{45}Ti (Figures 5A and 7, Table S4), which could indicate a relatively lower radiostability of ^{45}Ti-transferrin compared with [^{45}Ti]MSN-PEG$_{5k}$. Although the current silica-based ^{45}Ti radiolabeling is not designed for labeling ^{45}Ti to free antibody or peptides, it might still be quite useful given that silica surface modification has been widely used in developing multifunctional nanostructures[35, 36]. In addition, considering that ultrasmall (6–7 nm sized) renal clearable Cornell dots (which have been approved by the US Food and Drug Administration as Investigational New Drug for the first-in-human clinical trial studies) are also based on silica[37, 38], the developed ^{45}Ti (or ^{89}Zr) chelator-free radiolabeling technique might become a highly useful tool given that no extra chelator or surface modification is needed and size-controlling is vital when labeling these ultrasmall particles. Taken all together, we demonstrated the successful chelator-free ^{45}Ti radiolabeling to mesoporous silica nanoparticles and the potential use of [^{45}Ti]MSN-PEG$_{5k}$ for future biomedical applications.

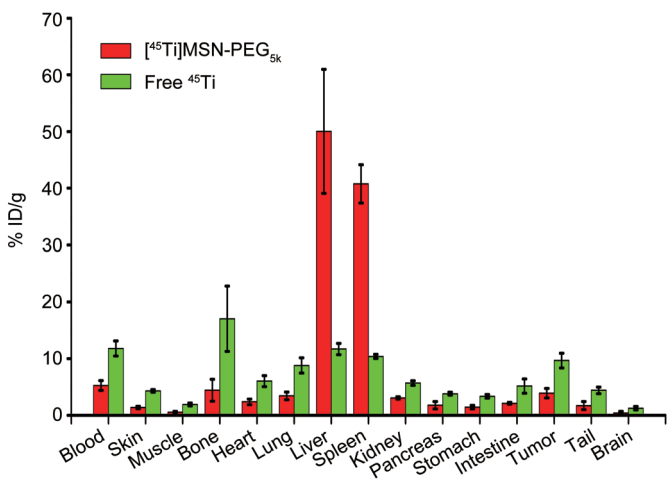

Figure 7. *Ex vivo* biodistribution of [^{45}Ti]MSN-PEG$_{5k}$ and free ^{45}Ti in 4T1 tumor-bearing mice at 20 and 18 h post-injection, respectively (n=3 for both groups).

In conclusion, an MSN-based intrinsic ^{45}Ti radiolabeling technique was developed. The mechanism was based on the strong interaction between ^{45}Ti (hard Lewis acid) and the hard oxygen donors (hard Lewis bases) of the deprotonated silanol groups from the outer surface and inner meso-channels of MSN. Successful chelator-free ^{45}Ti radiolabeling might also be achievable using other oxygen-containing nanoparticles. We hope these findings inspire researchers in the field of nano-oncology to create other ^{45}Ti-based multifunctional nanomedicine.

Supplementary information

Supplementary Figures and Tables are available at the website of Acta Pharmacologica Sinica.

Acknowledgements

This work is supported in part by the University of Wisconsin-Madison, the National Institutes of Health (NIBIB/NCI 1R01CA169365, P30CA014520, and 5T32GM08349), the National Science Foundation (No DGE-1256259), and the American Cancer Society (No 125246-RSG-13-099-01-CCE).

Author contribution

The manuscript was written by Feng CHEN, Hector F VALDOVINOS, and Wei-bo CAI. All authors have given approval to the final version of the manuscript. Feng CHEN, and Hector F VALDOVINOS contributed equally to this work.

References

1 Gambhir SS. Molecular imaging of cancer with positron emission tomography. Nat Rev Cancer 2002; 2: 683–93.
2 Cai W, Chen X. Multimodality molecular imaging of tumor angiogenesis. J Nucl Med 2008; 49 Suppl 2: 113s–28s.
3 Wadas TJ, Wong EH, Weisman GR, Anderson CJ. Coordinating radio-

metals of copper, gallium, indium, yttrium, and zirconium for PET and SPECT imaging of disease. Chem Rev 2010; 110: 2858–902.
4 Goel S, Chen F, Ehlerding EB, Cai W. Intrinsically radiolabeled nanoparticles: an emerging paradigm. Small 2014; 10: 3825–30.
5 Sun X, Cai W, Chen X. Positron emission tomography imaging using radiolabeled inorganic nanomaterials. Acc Chem Res 2015; 48: 286–94.
6 Chen F, Ellison PA, Lewis CM, Hong H, Zhang Y, Shi S, *et al.* Chelator-free synthesis of a dual-modality PET/MRI agent. Angew Chem Int Ed Engl 2013; 52: 13319–23.
7 Chakravarty R, Valdovinos HF, Chen F, Lewis CM, Ellison PA, Luo H, *et al.* Intrinsically germanium-69-labeled iron oxide nanoparticles: synthesis and *in-vivo* dual-modality PET/MR imaging. Adv Mater 2014; 26: 5119–23.
8 Sun X, Huang X, Guo J, Zhu W, Ding Y, Niu G, *et al.* Self-illuminating ^{64}Cu-doped CdSe/ZnS nanocrystals for *in vivo* tumor imaging. J Am Chem Soc 2014; 136: 1706–9.
9 Chen F, Goel S, Valdovinos HF, Luo H, Hernandez R, Barnhart TE, *et al. In vivo* integrity and biological fate of chelator-free zirconium-89-labeled mesoporous silica nanoparticles. ACS Nano 2015; 9: 7950–9.
10 Guo W, Sun X, Jacobson O, Yan X, Min K, Srivatsan A, *et al.* Intrinsically radioactive [^{64}Cu]CuInS/ZnS quantum dots for PET and optical imaging: improved radiochemical stability and controllable Cerenkov luminescence. ACS Nano 2015; 9: 488–95.
11 Rieffel J, Chen F, Kim J, Chen G, Shao W, Shao S, *et al.* Hexamodal imaging with porphyrin-phospholipid-coated upconversion nanoparticles. Adv Mater 2015; 27: 1785–90.
12 Shi S, Fliss BC, Gu Z, Zhu Y, Hong H, Valdovinos HF, *et al.* Chelator-free labeling of layered double hydroxide nanoparticles for *in vivo* PET imaging. Sci Rep 2015; 5: 16930.
13 Zhou M, Li J, Liang S, Sood AK, Liang D, Li C. CuS Nanodots with ultrahigh efficient renal clearance for positron emission tomography imaging and image-guided photothermal therapy. ACS Nano 2015; 9: 7085–96.
14 Buettner KM, Valentine AM. Bioinorganic chemistry of titanium. Chem Rev 2012; 112: 1863–81.
15 Ishiwata K, Ido T, Monma M, Murakami M, Kameyama M, Fukuda H, *et al*. Preparation of ^{45}Ti-labeled compounds and their medical application. J Labelled Comp Radiopharm 1982; 19: 1539–41.
16 Kawamura M, Inoue K, Kimura S, Ido T, Ishiwata K, Kawashima K, *et al*. Metabolism of ^{45}Ti-labeled compounds: effect of ascorbic acid. J Labelled Comp Radiopharm 1986; 23: 1360–62.
17 Ishiwata K, Ido T, Monma M, Murakami M, Fukuda H, Kameyama M, *et al.* Potential radiopharmaceuticals labeled with titanium-45. Int J Rad Appl Instrum A 1991; 42: 707–12.
18 Vavere AL, Laforest R, Welch MJ. Production, processing and small animal PET imaging of titanium-45. Nucl Med Biol 2005; 32: 117–22.
19 Vavere AL, Welch MJ. Preparation, biodistribution, and small animal PET of ^{45}Ti-transferrin. J Nucl Med 2005; 46: 683–90.
20 Severin GW, Nielsen CH, Jensen AI, Fonslet J, Kjaer A, Zhuravlev F. Bringing radiotracing to titanium-based antineoplastics: solid phase radiosynthesis, PET and *ex vivo* evaluation of antitumor agent [^{45}Ti](salan)Ti(dipic). J Med Chem 2015; 58: 7591–5.
21 Chen Y, Chen H, Shi J. *In vivo* bio-safety evaluations and diagnostic/therapeutic applications of chemically designed mesoporous silica nanoparticles. Adv Mater 2013; 25: 3144–76.
22 Yang P, Gai S, Lin J. Functionalized mesoporous silica materials for controlled drug delivery. Chem Soc Rev 2012; 41: 3679–98.
23 Zhou M, Zhang R, Huang M, Lu W, Song S, Melancon MP, *et al.* A chelator-free multifunctional [^{64}Cu]CuS nanoparticle platform for simultaneous micro-PET/CT imaging and photothermal ablation therapy. J Am Chem Soc 2010; 132: 15351–8.
24 Chen F, Hong H, Goel S, Graves SA, Orbay H, Ehlerding EB, *et al. In vivo* tumor vasculature targeting of CuS@MSN based theranostic nanomedicine. ACS Nano 2015; 9: 3926–34.
25 Hong H, Zhang Y, Severin GW, Yang Y, Engle JW, Niu G, *et al.* Multimodality imaging of breast cancer experimental lung metastasis with bioluminescence and a monoclonal antibody dual-labeled with 89Zr and IRDye 800CW. Mol Pharm 2012; 9: 2339–49.
26 Gagnon K, Severin GW, Barnhart TE, Engle JW, Valdovinos HF, Nickles RJ. ^{45}Ti extraction using hydroxamate resin. AIP Conference Proceedings 2012; 1509: 211–4.
27 Holland JP, Sheh Y, Lewis JS. Standardized methods for the production of high specific-activity zirconium-89. Nucl Med Biol 2009; 36: 729–39.
28 Valdovinos HF, Hernandez R, Barnhart TE, Graves S, Cai W, Nickles RJ. Separation of cyclotron-produced 44Sc from a natural calcium target using a dipentyl pentylphosphonate functionalized extraction resin. Appl Radiat Isot 2015; 95: 23–9.
29 Burrows TW. Nuclear data sheets for A=45. Nuclear Data Sheets 2008; 109: 171–296.
30 Shen D, Yang J, Li X, Zhou L, Zhang R, Li W, *et al*. Biphase stratification approach to three-dimensional dendritic biodegradable mesoporous silica nanospheres. Nano Lett 2014; 14: 923–32.
31 Goel S, Chen F, Luan S, Valdovinos HF, Shi S, Graves SA, *et al*. Engineering intrinsically zirconium-89 radiolabeled self-destructing mesoporous silica nanostructures for *in vivo* biodistribution and tumor targeting studies. Adv Sci (Weinh) 2016; 3: 1600122.
32 1Guo M, Sun H, McArdle HJ, Gambling L, Sadler PJ. Ti(IV) uptake and release by human serum transferrin and recognition of Ti(IV)-transferrin by cancer cells: understanding the mechanism of action of the anticancer drug titanocene dichloride. Biochemistry 2000; 39: 10023–33.
33 Sun H, Li H, Weir RA, Sadler PJ. The first specific tiiv-protein complex: potential relevance to anticancer activity of titanocenes. Angew Chem Int Ed Engl 1998; 37: 1577–9.
34 Fang J, Nakamura H, Maeda H. The EPR effect: Unique features of tumor blood vessels for drug delivery, factors involved, and limitations and augmentation of the effect. Adv Drug Deliv Rev 2011; 63: 136–51.
35 Zhang Y, Hsu BY, Ren C, Li X, Wang J. Silica-based nanocapsules: synthesis, structure control and biomedical applications. Chem Soc Rev 2015; 44: 315–35.
36 Bitar A, Ahmad NM, Fessi H, Elaissari A. Silica-based nanoparticles for biomedical applications. Drug Discov Today 2012; 17: 1147–54.
37 Benezra M, Penate-Medina O, Zanzonico PB, Schaer D, Ow H, Burns A, *et al.* Multimodal silica nanoparticles are effective cancer-targeted probes in a model of human melanoma. J Clin Invest 2011; 121: 2768–80.
38 Phillips E, Penate-Medina O, Zanzonico PB, Carvajal RD, Mohan P, Ye Y, *et al.* Clinical translation of an ultrasmall inorganic optical-PET imaging nanoparticle probe. Sci Transl Med 2014; 6: 260ra149.